

# Forecasting Constraints on Non-Thermal Light Massive Relics from Future CMB Experiments

Arka Banerjee,<sup>1</sup> Abhik Bhattacharjee,<sup>2,\*</sup> Subinoy Das,<sup>3</sup> Anshuman Maharana,<sup>2</sup> and Ravi Kumar Sharma<sup>4,†</sup>

<sup>1</sup>*Department of Physics, Indian Institute of Science Education and Research, Homi Bhabha Road, Pashan, Pune 411008, India*

<sup>2</sup>*Harish-Chandra Research Institute, A CI of Homi Bhabha National Institute, Chhatnag Road, Jhansi, Prayagraj, Uttar Pradesh 211019, India*

<sup>3</sup>*Indian Institute of Astrophysics, Bengaluru, Karnataka 560034, India*

<sup>4</sup>*Institute for Theoretical Particle Physics and Cosmology (TTK), RWTH Aachen University, Sommerfeldstr. 16, D-52056 Aachen, Germany*

Precise measurements of the cosmological impact of dark sector relics can shed light on Physics beyond the Standard Model. In this work we present Fisher forecasts on *non-thermal LiMR* models for the upcoming CMB Stage IV experiment—particularly focusing on a model of inflaton/moduli decay giving rise to non-thermally distributed dark sector particles, and also comparing our results with those for sterile particles following the Dodelson-Widrow distribution. Two independent parameters, the effective number of extra relativistic species  $\Delta N_{\text{eff}}$  and the effective mass  $M_{\text{sp}}^{\text{eff}}$  of the relic, influence linear cosmological observables. We find  $\Delta N_{\text{eff}}$  to be more tightly constrained with  $\sigma(\Delta N_{\text{eff}}) \sim 10^{-3}$ , for a less abundant, heavier LiMR which becomes fully non-relativistic around matter-radiation equality than a more abundant, lighter LiMR which becomes fully non-relativistic just after recombination, for which  $\sigma(\Delta N_{\text{eff}}) \sim 10^{-2}$ . The uncertainties on  $M_{\text{sp}}^{\text{eff}}$  differ by a factor of  $\sim 3$  between the two cases. Our analysis also reveals distinct parameter correlations: the phenomenological parameters  $\{\Delta N_{\text{eff}}, M_{\text{sp}}^{\text{eff}}\}$  are found to be negatively correlated for the former case and positively correlated for the latter. We obtain similar constraints on the cosmological parameters (in either case) for both the inflaton/moduli decay and the Dodelson-Widrow models when the first two moments of the LiMR distribution function, related to the phenomenological parameters, are matched. Finally, by constructing a modified distribution that matches the first two moments of the Dodelson-Widrow but deviates maximally in the third moment, we demonstrate that CMB Stage IV data is not expected to be sensitive to higher moments of the distribution.

## I. INTRODUCTION

The Cosmic Microwave Background (CMB) provides a snapshot of the Universe at the time of recombination – when electrons and protons combined to form hydrogen atoms – which occurred about 380, 000 years after the end of inflation. Post recombination, photons decoupled from the cosmic plasma giving rise to the CMB. Likewise, neutrinos decoupled from the plasma when the expansion rate of the universe exceeded the rate of weak interactions, when the Universe was about a second old. This gave rise to the Cosmic Neutrino Background (C $\nu$ B), which has not been detected yet, but analysis of CMB anisotropies [e.g. 1–3] and agreement between calculated and observed primordial abundances of light elements indirectly establishes its presence [4]. An important observable in any cosmological model is the energy density in radiation at the time of recombination. Within the Standard Model (SM), photons and neutrinos are the sole contributors to this. More generally, with Beyond the Standard Model (BSM) physics, there can be contributions from other species. Observational results are usually reported by making use of the quantity  $N_{\text{eff}}$ , the effective number of neutrino like species contributing to

the radiation energy density before photon decoupling, in addition to that of photons. Current constraints on  $N_{\text{eff}}$  from CMB measurements are  $2.99 \pm 0.17$  (68% CL; Planck TT,TE,EE+lensing+BAO) [5] and  $N_{\text{eff}} < 3.08$  (one tail 95%; P-ACT-LB) [6], which are consistent with the SM prediction of  $N_{\text{eff}} = 3.044$  [7–9]. However, there is still room for  $\Delta N_{\text{eff}} \equiv N_{\text{eff}} - 3.044 \neq 0$  once we include recent BAO measurements from DESI DR2:  $N_{\text{eff}} = 3.10 \pm 0.17$  (68% CL; DESI+CMB) [10] and  $N_{\text{eff}} = 3.23 \pm 0.18$  (68% CL; DESI BAO+CMB) [11]. So the possibility of the existence of extra relativistic particles is not ruled out yet. Furthermore,  $N_{\text{eff}}$  will be probed with even greater precision with future CMB experiments. The upcoming CMB Stage IV (CMB-S4) survey has been designed to have far better sensitivity to  $N_{\text{eff}}$  with a target of  $\sigma(N_{\text{eff}}) = 0.02 - 0.03$  for the  $\Lambda$ CDM model extended by  $N_{\text{eff}}$  [12]. A quantitative understanding of possible constraints on theoretical models with the expected data quality from CMB-S4 is timely.

The presence of new light relics which behave as “dark radiation” and contribute to  $\Delta N_{\text{eff}}$ , is a generic feature of many BSM proposals. Sources for dark radiation include sterile neutrinos [e.g. 13–15], and axions [e.g. 16–19], among others<sup>1</sup>. Certain studies propose the existence of sterile neutrinos [20–22] to address anomalies in

\* abhikbhattacharjee@hri.res.in

† rksharma@physik.rwth-aachen.de

<sup>1</sup> See Ref. [12] (and references therein) for discussion of other pos-

neutrino oscillation data [23, 24]. In spite of the particle physics motivation, a fully thermalized fourth sterile neutrino which decoupled along with the standard neutrinos is ruled out due to stringent constraints on  $N_{\text{eff}}$  mentioned above [5]. Models with more complicated structures for the neutrino sector have also been proposed [e.g. 25], and possible constraints from cosmological data have been investigated [26]. However, hot thermal relics which decoupled from the SM plasma at an earlier time than neutrino decoupling could be exempted from the strong constraints on  $N_{\text{eff}}$ . Thermal relics with decoupling temperatures above the top quark mass have the following minimal contributions:  $\Delta N_{\text{eff}} = 0.027$  for a Goldstone boson,  $\Delta N_{\text{eff}} = 0.047$  for a Weyl fermion, and  $\Delta N_{\text{eff}} = 0.054$  for vector boson [27]. The cosmological impact of such massless light relics (or relics with masses  $m \ll \text{eV}$ ) is completely captured by the  $N_{\text{eff}}$  parameter [16]. They primarily affect the expansion of the Universe, causing a suppression of the damping tail of the CMB power spectrum as well as a phase shift in the Baryon Acoustic Oscillations [1, 16, 19, 28, 29].

The other possibility is that of Light Massive Relics (LiMRs) — massive particles which contributed to the radiation energy density in the early Universe and to the matter energy density at late times. The LiMR mass is an important parameter as it controls the time at which the LiMR transitions to being non-relativistic, after which it behaves as a sub-component of the total Dark Matter (DM) component of the Universe. Increasing the effective mass of the LiMR primarily affects the CMB power spectrum at low multipoles through the late Integrated Sachs-Wolfe (ISW) effect and CMB lensing [4, 30, 31]. In Ref. [32], the authors combined CMB and LSS data to obtain limits on the masses of thermally decoupled species  $X$  (with a present day temperature of  $T_X^{(0)} = 0.91 \text{ K}$ ):  $m_X \leq 11, 2.3, 1.6 \text{ eV}$  for scalars, Weyl fermions, and vectors respectively. Fisher forecasts for such LiMRs, with masses ranging from  $10^{-2} \text{ eV} \leq m_X \leq 10 \text{ eV}$  and temperatures in the range [0.91 K, 1.50 K], have been performed in Ref. [33] to obtain constraints on  $g_X$ , the number of degrees of freedom of the LiMR, from the CMB-S4 experiment.

While much of the literature has focused on thermal relics, this paper deals with LiMRs in *non-thermal* distributions. Various well-motivated models have been proposed to generate species with non-thermal distributions in the early Universe. One of the familiar categories is through mixing of active neutrinos [34, 35], while another is through the decay of heavy particles in the early Universe [36–40]. Belonging to the later category is the perturbative decay of the inflaton [41] or the decay of the moduli due to vacuum misalignment (see, for instance, Ref. [42]). We focus on two concrete examples of such distributions to draw out the main features: the first

arises from the inflaton/moduli decay in the early Universe [e.g. 37, 40]. The second distribution we examine is the Dodelson-Widrow distribution [34], originally proposed for sterile neutrinos. We perform Fisher forecasts for these models to quantify the constraints on their parameters that are expected from a survey with the specifications of the CMB-S4 experiment. We also investigate how features of the shape of the LiMR distribution function can affect observables.

The paper is structured as follows: Section II gives a brief review of some basic aspects of the LiMR models, Fisher forecasts and future experimental prospect. We discuss our implementation in section III. Our results are presented in Section IV. In Section V, we discuss the effect of the shape of the distribution function. We conclude in Section VI.

## II. REVIEW

### A. Light Massive relics

We begin by discussing some general aspects of LiMR models. The influence of LiMRs on linear cosmological observables can be characterized by three parameters (see Ref. [43] for details).

- $\Delta N_{\text{eff}}$ : This parameter represents the contribution of LiMRs to the Universe’s relativistic energy density before photon decoupling. It is defined as ( $g_s$  is a degeneracy factor):

$$\Delta N_{\text{eff}} \equiv \frac{\rho_{\text{sp}}^{\text{rel}}}{\rho_\nu} = \frac{g_s}{7/4} \left[ \frac{1}{\pi^2} \int dp p^3 \hat{f}(p) \right] / \left[ \frac{7\pi^2}{120} (T_\nu^{\text{id}})^4 \right], \quad (1)$$

where  $\hat{f}(p)$  is the momentum distribution function of the LiMR, and  $T_\nu^{\text{id}} \equiv (4/11)^{1/3} T_\gamma$  is the neutrino temperature in terms of the photon temperature, assuming instantaneous neutrino decoupling.

- $M_{\text{sp}}^{\text{eff}}$ : This parameter represents the contribution of the LiMR to the Universe’s current energy density, and it is defined as ( $g'_s$  is a degeneracy factor):

$$\frac{M_{\text{sp}}^{\text{eff}}}{94.05 \text{ eV}} \equiv \omega_{\text{sp}} = \frac{g'_s}{3/2} \left[ \frac{m_{\text{sp}}}{\pi^2} \int dp p^2 \hat{f}(p) \right] \left[ \frac{h^2}{\rho_{\text{crit}}^0} \right], \quad (2)$$

where  $h$  is the reduced Hubble constant and  $\rho_{\text{crit}}^0$  denotes the critical density of the Universe today.

- $\langle v_{\text{fs}} \rangle$ : The typical free-streaming velocity of the particles today, given by

$$\langle v_{\text{fs}} \rangle \equiv \frac{\frac{g_s}{7/4} \int dp p^2 \frac{p}{m_{\text{sp}}} \hat{f}(p)}{\frac{g'_s}{3/2} \int dp p^2 \hat{f}(p)} = 5.236 \times 10^{-4} \frac{\Delta N_{\text{eff}}}{M_{\text{sp}}^{\text{eff}}}. \quad (3)$$

Note that only two of the three parameters are independent. In our study, we will utilize  $M_{\text{sp}}^{\text{eff}}$  and  $\Delta N_{\text{eff}}$  as

---

sibilities and their prospects for detection by the CMB-S4 experiment.

phenomenological parameters to investigate the impact of LiMRs. Also, the above described parameters are determined by the first two moments of the distribution function. We will examine the role of higher moments in section V. Note that the parameter  $g_X$  of Ref. [32] is related to our  $g_s, g'_s$ . But unlike in Ref. [32], where the constraints on  $\Delta N_{\text{eff}}$  or  $M_{\text{sp}}^{\text{eff}}$  (equivalently  $\Omega_X$ ) were obtained by translating the constraints on  $g_X$ , here we shall find the uncertainties on these phenomenological parameters by varying the mass  $m_{\text{sp}}$  and a model specific parameter (see below) which enters into the momentum distribution function.

Next, we describe the two LiMR distribution functions that we will consider in the paper.

### 1. Distribution function associated with production via decay of the Inflaton/Moduli

During reheating after inflation or an epoch of moduli domination, the early Universe can go through a matter-dominated era with its energy density dominated by heavy cold particles ( $\phi$ ). In addition to the decay to the SM sector, the  $\phi$  particle can decay to a LiMR in the dark sector. This typically occurs via a  $1 \rightarrow 2$  process:

$$\phi \xrightarrow{B_{\text{sp}}} \mathbf{x}\mathbf{x},$$

where  $\mathbf{x}$  stands for the LiMR. The production rate of  $\mathbf{x}$  is controlled by the decay lifetime  $\tau$ , the mass  $m_\phi$ , and the branching ratio  $B_{\text{sp}}$ . LiMRs produced via this mechanism have the following momentum distribution (as given in Ref. [40]; see Appendix A for further details):

$$f(\mathbf{q}) = \frac{32}{\pi \hat{E}^3} \left( \frac{N(0)B_{\text{sp}}}{\hat{s}^3(\theta^*)} \right) \frac{\exp(-\hat{s}^{-1}(y))}{|\mathbf{q}|^3 \hat{H}(\hat{s}^{-1}(y))}. \quad (4)$$

Here  $y = (|\mathbf{q}|/4)\hat{s}(\theta^*)$ ,  $\hat{E}$  is the energy of the particles at production,  $N(0)$  is the initial number density of the  $\phi$  particles,  $\hat{s}(\theta^*) \equiv a(t^*)$  is the scale factor as a function of dimensionless time  $\theta$  (with  $\theta^*$  indicating the time by which all the  $\phi$  particles have decayed),  $\hat{s}^{-1}$  is the functional inverse of the scale factor function, and  $\hat{H} = \hat{s}'(\theta)/\hat{s}(\theta)$  is the dimensionless Hubble parameter.

The model has four microscopic parameters:  $m_\phi, \tau, B_{\text{sp}}$  and  $m_{\text{sp}}$ . We will take the first two parameters to be  $m_\phi \sim 10^{-6} M_{\text{pl}}$  and  $\tau \sim 10^8/m_\phi$  (motivated by having  $\phi$  to be driving inflation at the GUT scale and decaying by GUT scale interactions). The phenomenological parameters  $\{\Delta N_{\text{eff}}, M_{\text{sp}}^{\text{eff}}\}$  are related to the model parameters by the following expressions [40]:

$$\Delta N_{\text{eff}} = \frac{43}{7} \frac{B_{\text{sp}}}{1 - B_{\text{sp}}} \left( \frac{g_*(T(t_\nu))}{g_*(T(t^*))} \right)^{1/3}, \quad (5)$$

$$M_{\text{sp}}^{\text{eff}} = \frac{62.1 m_{\text{sp}}}{g_*^{1/4}(T(t^*))} \frac{B_{\text{sp}}}{(1 - B_{\text{sp}})^{3/4}} \left( \frac{M_{\text{pl}}}{\tau m_\phi^2} \right)^{1/2}, \quad (6)$$

where  $t_\nu$  is the neutrino-decoupling time and  $g_*(T(t))$  is the effective number of degrees of freedom at a temperature  $T$  (corresponding to a time  $t$ ).

### 2. The Dodelson-Widrow Distribution

We also consider the Dodelson-Widrow distribution [34]. Non-resonant active-sterile neutrino oscillations in the early Universe in the limit of small mixing angle leads to the following distribution function for the sterile neutrinos:

$$f_\nu(p) = \frac{\chi}{e^{p/T_\nu} + 1}, \quad (7)$$

where  $\chi$  is an arbitrary normalization factor and  $T_\nu$  is the temperature of neutrinos today. With  $T_\nu = T_\nu^{\text{id}}$ , the phenomenological parameters are related to the model parameters via the following relations:

$$\Delta N_{\text{eff}} = \chi \quad \text{and} \quad M_{\text{sp}}^{\text{eff}} = m_{\text{sp}} \times \chi, \quad (8)$$

where  $m_{\text{sp}}$  is the mass of the sterile neutrinos.

## B. Fisher Forecast Methodology

### 1. Formalism

Suppose we have a set of data  $\{\mathbf{d}\}$  and a model  $\mathcal{M}$  with a set of parameters  $\{\boldsymbol{\theta}\}$ . We want to find the probability distribution of  $\{\boldsymbol{\theta}\}$ , given the data  $\{\mathbf{d}\}$ , i.e.,  $P(\boldsymbol{\theta}|\mathbf{d})$ , which is obtained using Bayes' theorem:

$$P(\boldsymbol{\theta}|\mathbf{d}) \propto P(\mathbf{d}|\boldsymbol{\theta})P(\boldsymbol{\theta}) \quad (9)$$

Here  $P(\boldsymbol{\theta})$  and  $P(\boldsymbol{\theta}|\mathbf{d})$  are called the *prior* and *posterior* distributions respectively and  $P(\mathbf{d}|\boldsymbol{\theta})$  is called the *Likelihood*, usually denoted by  $\mathcal{L}$ , and can be expressed as follows:

$$\mathcal{L}(\mathbf{d}; \boldsymbol{\theta}) = \frac{1}{\sqrt{\mathbf{C}(\boldsymbol{\theta})}} \exp(-\mathbf{d}^T \mathbf{C}(\boldsymbol{\theta}) \mathbf{d}), \quad (10)$$

where  $\mathbf{C}$  represents the covariance matrix. The Fisher matrix is related to the curvature of the log-likelihood function, evaluated at the fiducial values of the parameters:

$$F_{ij} = - \left\langle \frac{\partial^2 \ln \mathcal{L}}{\partial \theta_i \partial \theta_j} \right\rangle \Big|_{\boldsymbol{\theta}=\boldsymbol{\theta}_0}, \quad (11)$$

$\theta_i, \theta_j$  being the parameters of interest and  $\boldsymbol{\theta}_0$  being the fiducial set of parameters [44].

*Derived Parameters:* If we have a Fisher matrix in terms of a set of parameters  $\{\boldsymbol{\theta}\}$ , we can obtain a new Fisher matrix in terms of a set of derived parameters  $\{\boldsymbol{\theta}'\}$  as [45]

$$F' = J^T \cdot F \cdot J, \quad (12)$$

where  $J$  stands for the inverse Jacobian matrix  $\partial\theta/\partial\theta'$ . This will be used, for instance, to translate the  $1\sigma$  uncertainties on  $\{B_{\text{sp}}, m_{\text{sp}}\}$  to those on  $\{\Delta N_{\text{eff}}, M_{\text{sp}}^{\text{eff}}\}$ .

*Error Estimate:* After computing the Fisher information matrix, we can derive the error covariance matrix by taking its inverse

$$\text{Cov}_{ij} = (F^{-1})_{ij}. \quad (13)$$

The diagonal elements of the error covariance matrix indicate the marginalized errors on the parameters. For instance, the anticipated marginalized  $1\sigma$  error on a parameter  $\theta_i$ , accounting for all degeneracies concerning other parameters, is calculated as:

$$\sigma_i^{(\text{marg.})} = \sqrt{\text{Cov}_{ii}}. \quad (14)$$

The unmarginalized expected errors, or conditional errors, can be determined by

$$\sigma_i^{(\text{cond.})} = \sqrt{\frac{1}{F_{ii}}}, \quad (15)$$

representing the square root of the reciprocal of the relevant diagonal element of the Fisher matrix.

*Posterior Probability or confidence regions:* For the form of the Likelihood function (10), the posterior probability is Gaussian (under the Fisher assumption<sup>2</sup>) with the  $1\sigma$  and  $2\sigma$  intervals encompassing 68.3% and 95.4% of the total probability respectively. For Gaussian posterior, the confidence regions are ellipses in the parameter space, whose size and orientation are determined by the Fisher matrix elements. Confidence regions correspond to regions in parameter space in which the joint parameter values are expected to lie with a certain probability –  $1\sigma$  region corresponds to 39.35% probability and  $2\sigma$  region corresponds to 86.47% probability.

## 2. CMB Experiments

In the context of Cosmic Microwave Background (CMB), the data vector is either the CMB power spectra or spherical harmonic coefficients represented as  $\mathbf{d} = \{a_{\ell m}^T, a_{\ell m}^E, a_{\ell m}^\phi\}$ . The Fisher information matrix takes the following form [46]:

$$F_{ij} = \sum_{\ell} \frac{2\ell + 1}{2} f_{\text{sky}} \text{Tr} \left( \mathbf{C}_{\ell}^{-1}(\boldsymbol{\theta}) \frac{\partial \mathbf{C}_{\ell}}{\partial \theta_i} \mathbf{C}_{\ell}^{-1}(\boldsymbol{\theta}) \frac{\partial \mathbf{C}_{\ell}}{\partial \theta_j} \right), \quad (16)$$

where  $f_{\text{sky}}$  is the fractional sky coverage,  $\boldsymbol{\theta}$  represents the vector of parameters, and  $\mathbf{C}_{\ell}$  is the total covariance

matrix of the relevant CMB observables (temperature, E-mode polarization, and lensing potential) given by [47]:

$$\mathbf{C}_{\ell} = \begin{pmatrix} C_{\ell}^{TT} + N_{\ell}^{TT} & C_{\ell}^{TE} & C_{\ell}^{T\phi} \\ C_{\ell}^{TE} & C_{\ell}^{EE} + N_{\ell}^{EE} & 0 \\ C_{\ell}^{T\phi} & 0 & C_{\ell}^{\phi\phi} + N_{\ell}^{\phi\phi} \end{pmatrix}$$

This includes the Gaussian noise  $N_{\ell}^{XX}$ , where  $XX \in \{TT, EE\}$ , given by [12]

$$N_{\ell}^{XX} = s^2 \exp \left( \ell(\ell + 1) \frac{\theta_{\text{FWHM}}^2}{8 \ln 2} \right), \quad (17)$$

where  $\theta_{\text{FWHM}}$  is the resolution of the experiment in arcmin, and  $s$  is the instrumental noise in temperature/polarization.

## III. IMPLEMENTATION

The  $C_{\ell}$ 's appearing in the total covariance matrix  $\mathbf{C}_{\ell}$  above were obtained from the publicly available package CLASS<sup>3</sup> [48], suitably modified to incorporate the non-thermal distribution functions under consideration [49]. The noise properties for the experiments considered in this work are listed in Table I [12, 50], and the TT and EE noise spectra were computed using Eq. (17) with these noise parameters. For the lensing convergence, we used the orphics<sup>4</sup> code [51] to calculate the noise spectrum  $N_{\ell}^{\kappa\kappa}$  (subsequently converted to  $N_{\ell}^{\phi\phi}$ ) from a minimum variance combination of  $TT, TE, EE, EB$ , and  $TB$  quadratic estimators, assuming the CMB B-modes undergo an iterative delensing procedure. Following the CMB-S4 Science Book [12], we have set  $\ell_{\text{min}} = 30$  (recovering large scales from ground is challenging), and  $\ell_{\text{max}}^T = 3000$  and  $\ell_{\text{max}}^P = 5000$  for CMB-S4 (due to foregrounds). For Planck, we have considered  $2 < \ell^T < 2500$  and  $30 < \ell^P < 2500$ . For the lensing signal, we have considered  $30 < \ell^{\phi} < 2500$ . We have assumed infinite noise outside these multipole ranges [50] and have set the derivatives of the  $C_{\ell}$ 's to zero outside the corresponding multipole ranges to ignore their contribution to our analysis<sup>5</sup>. When analyzing  $C_{\ell}^{TT}, C_{\ell}^{TE}, C_{\ell}^{EE}$  in combination with the lensing convergence spectra  $C_{\ell}^{\phi\phi}$  (which has been assumed to contain all the lensing information), we have used unlensed  $C_{\ell}$ 's in our Fisher analysis in order to avoid double-counting lensing information [50].

Measurements of CMB-S4 are usually considered in combination with Planck data because the two experiments are highly complementary. Planck, as a satellite

<sup>2</sup> One can have non-Gaussian posteriors in general even for a Gaussian likelihood when priors are non-Gaussian.

<sup>3</sup> <https://github.com/lesgourg/class-public>

<sup>4</sup> <https://github.com/msyriac/orphics>

<sup>5</sup> See Appendix B for a discussion on numerical derivatives.

Experiment	$\ell$ range	Noise $s[\mu\text{K} - \text{arcmin}]$	$f_{\text{sky}}$	$\theta_{\text{FWHM}}[\text{arcmin}]$
Planck	T: 2 – 2500	T: [145, 149, 137, 65, 43, 66, 200]	0.6	[33, 23, 14, 10, 7, 5, 5]
	P: 30 – 2500	P: [–, –, 450, 103, 81, 134, 406]		
CMB-S4	T: 30 – 3000	T: 1.0	0.4	1.5
	P: 30 – 5000	P: 1.414		
CV-limited	T/P: 2 – 5000	0.0	1.0	N/A

Table I: Experimental parameters for Planck and a particular configuration of the CMB-S4 experiment used for the Fisher analysis. We also considered a standalone, full-sky, cosmic-variance limited experiment.

mission, provides a higher sky coverage and can also capture the largest angular scales (low  $\ell$ 's). On the other hand, CMB-S4, being a ground-based experiment offers better sensitivity and precision on smaller angular scales (high  $\ell$ s). So for the Planck and CMB-S4 joint analysis, we added the corresponding Fisher matrices,

$$F = F^{\text{Planck}} + F^{\text{CMB-S4}}, \quad (18)$$

with the caveat that in the region of overlap between the two experiments, which is  $30 < \ell < 2500$ , we set  $f_{\text{sky}} = 0.2$  for Planck in order to avoid double-counting. We used flat priors for all parameters except  $\tau_{\text{reio}}$ , for which we have added a prior of 0.01 as follows [52]:

$$F_{ii} \rightarrow F_{ii} + \frac{1}{\text{prior}_i^2}. \quad (19)$$

We utilized the `fishchips` package<sup>6</sup> to develop our code for Fisher analysis.

#### IV. RESULTS

The fiducial model consists of the following six  $\Lambda\text{CDM}$  parameters: the physical baryon density  $\omega_b$ , the physical cold dark matter density  $\omega_{\text{cdm}}$ , the reduced Hubble constant  $h$ , the amplitude of primordial scalar perturbations  $A_s$ , the scalar spectral tilt  $n_s$ , and the optical depth to reionization  $\tau_{\text{reio}}$ , and the two phenomenological parameters  $\{\Delta N_{\text{eff}}, M_{\text{sp}}^{\text{eff}}\}$ . The phenomenological parameters are however derived parameters — related to the inflaton/moduli-decay-model parameters  $\{B_{\text{sp}}, m_{\text{sp}}\}$  (via Eqs. (5) and (6)) or the Dodelson-Widrow-model parameters  $\{\chi, m_{\text{sp}}\}$  (via Eq. (8)). For both these models, we assume Standard Model neutrinos to be massless as in Ref. [53] since the effect of neutrino masses is expected to be subdominant for the cosmological observables of interest. In Fig. 1, we plot the non-thermal (NT) distribution along with the Dodelson-Widrow (DW) distribution for the same values of the phenomenological parameters, viz.  $\Delta N_{\text{eff}} = 0.034$  and  $M_{\text{sp}}^{\text{eff}} = 0.903$  eV.

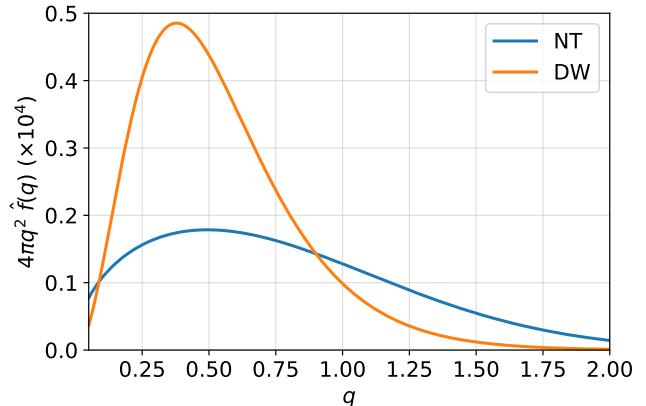


Figure 1: Comparative plot of the inflaton decay (NT) and Dodelson-Widrow (DW) distributions for  $\{\Delta N_{\text{eff}}, M_{\text{sp}}^{\text{eff}}\} = \{0.034, 0.903$  eV $\}$ . The momenta and the distribution function are both in units of  $T_{\text{ncdm},0}$  which is calculated using Eq. (A9) with  $m_\phi = 10^{-6} M_{\text{Pl}}$ ,  $\tau = 10^8/m_\phi$ , and  $B_{\text{sp}} = 0.0118$  for the NT model.

We have performed the Fisher analyses with two sets of fiducial values:

- Set I: We used the best fit of MCMC analysis with Planck 18+S8 data sets performed in Ref. [53] for the inflaton decay model. The fiducial values of the  $\nu_{\text{NT}}\Lambda\text{CDM}$  model parameters, corresponding to the fiducial values of the phenomenological parameters,  $\{\Delta N_{\text{eff}}, M_{\text{sp}}^{\text{eff}}\} = \{0.034, 0.903$  eV $\}$ , are

$$B_{\text{sp}} = 0.0118, \quad m_{\text{sp}} = 38.62 \text{ eV}, \quad (20)$$

whereas for the Dodelson-Widrow model, we have

$$\chi = 0.034, \quad m_{\text{sp}} = 26.43 \text{ eV}. \quad (21)$$

- Set II: We used the mean values of the  $\Lambda\text{CDM}$  parameters obtained from Planck TT, TE, EE+lens+low E+lensing when the base- $\Lambda\text{CDM}$  model is extended by including  $M_{\text{sp}}^{\text{eff}}$  and  $N_{\text{eff}}$  [5]. In this extension of the base  $\Lambda\text{CDM}$  model, the physical mass of a thermal sterile neutrino is  $m_{\text{sp}}^{\text{th}} =$

<sup>6</sup> <https://github.com/xzackli/fishchips-public>

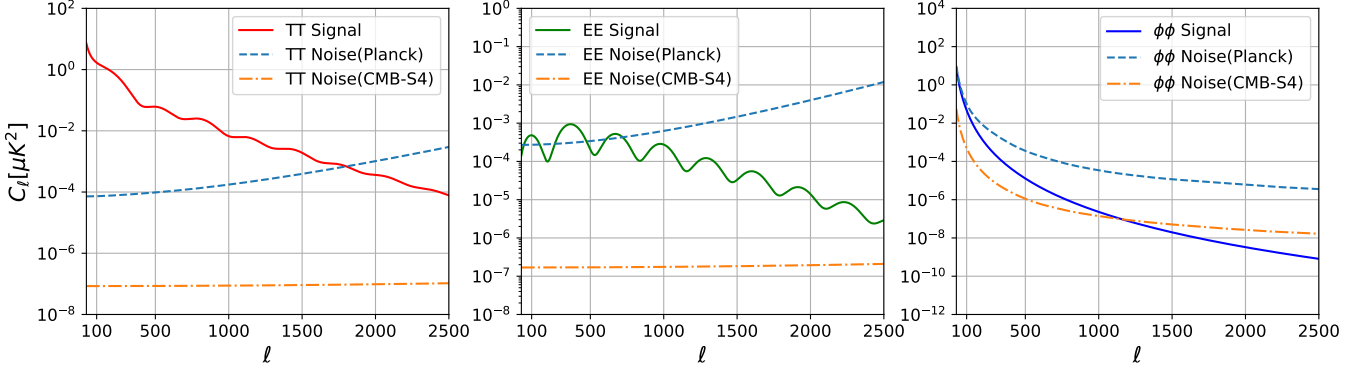


Figure 2: Plots of various auto-correlation signal and noise spectra for the inflaton/moduli decay model with the parameter values from Table II (set I).

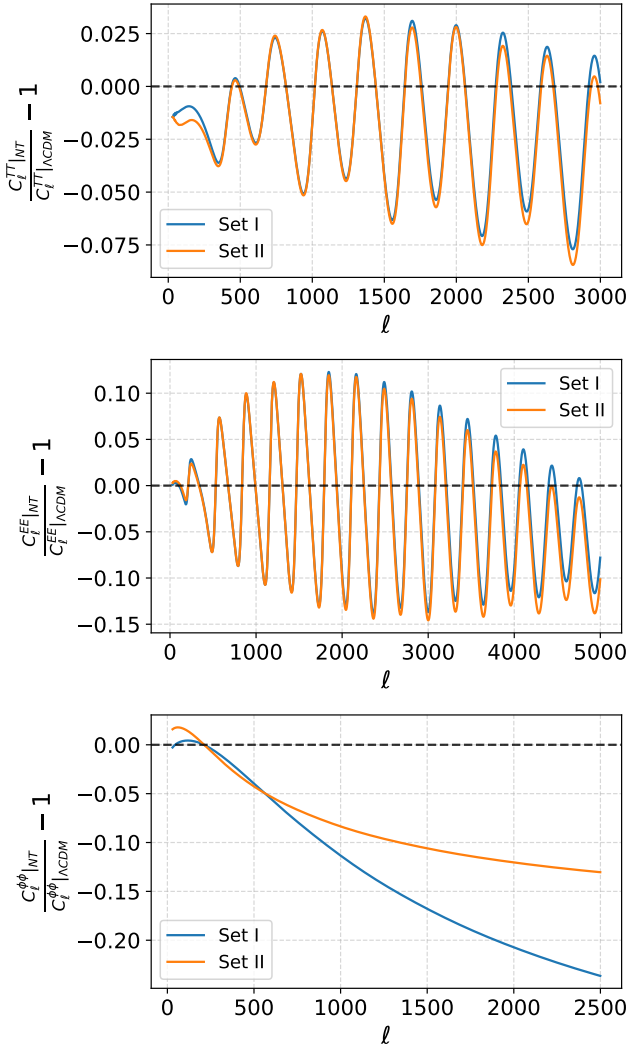


Figure 3: Comparison of the residuals of the TT, EE, and  $\phi\phi$  spectra for the two sets of fiducial values.

Parameter	Fiducial value	
	Set I	Set II
$\omega_b$	0.02247	0.02242
$\omega_{\text{cdm}}$	0.111	0.120
$h$	0.6804	0.6711
$10^9 A_s$	2.099	2.110
$n_s$	0.9661	0.9652
$\tau_{\text{reio}}$	0.0536	0.0560
$\Delta N_{\text{eff}}$	0.034	0.1
$M_{\text{sp}}^{\text{eff}}$ [eV]	0.903	0.4

Table II: Fiducial values used for Fisher analysis.

$(\Delta N_{\text{eff}})^{-3/4} M_{\text{sp}}^{\text{eff}}$ . Assuming the prior  $m_{\text{sp}}^{\text{th}} < 10$  eV, the Planck paper found the following  $2\sigma$  constraints on  $\Delta N_{\text{eff}}$  and  $M_{\text{sp}}^{\text{eff}}$  from Planck TT, TE, EE+low E+lensing+BAO,

$$\Delta N_{\text{eff}} < 0.246 \quad \text{and} \quad M_{\text{sp}}^{\text{eff}} < 0.65 \text{ eV}. \quad (22)$$

We chose  $\Delta N_{\text{eff}} = 0.1$  and  $M_{\text{sp}}^{\text{eff}} = 0.4$  eV, which corresponds to the following values of the model parameters:

$$B_{\text{sp}} = 0.0332, \quad m_{\text{sp}} = 6.2 \text{ eV}; \quad (23)$$

$$\chi = 0.1, \quad m_{\text{sp}} = 4.0 \text{ eV}. \quad (24)$$

The fiducial values of the  $\Lambda$ CDM parameters along with the phenomenological parameters  $\{\Delta N_{\text{eff}}, M_{\text{sp}}^{\text{eff}}\}$ , for both sets, are listed in Table II. Various auto-correlation spectra obtained from CLASS (and orphics) using the parameter values of set I for the inflaton/moduli decay model are plotted in Fig. 2, which also shows the improvements in the noise levels for CMB-S4 as compared to Planck. In Fig. 3 we show the comparative plots of  $C_\ell^{TT}$ ,  $C_\ell^{EE}$ , and  $C_\ell^{\phi\phi}$  for the two sets of fiducial values

Parameter	$10^5 \omega_b$	$10^3 \omega_{\text{cdm}}$	$H_0$	$\ln(10^{10} A_s)$	$n_s$	$\tau_{\text{reio}}$	$\Delta N_{\text{eff}}$	$M_{\text{sp}}^{\text{eff}}$ [eV]
$1\sigma$ error(CMB-S4)	2.85	1.26	0.263	0.010	0.0019	0.0059	0.0038	0.080
$1\sigma$ error(Planck+S4)	2.74	1.23	0.247	0.009	0.0018	0.0056	0.0037	0.080
$1\sigma$ error(CV-limited)	0.79	0.29	0.089	0.003	0.0008	0.0014	0.0013	0.012

Table III: Projected  $1\sigma$  errors for parameters  $\theta_i$ , marginalized over all other parameters for the inflaton-decay NT model with  $\{\Delta N_{\text{eff}}, M_{\text{sp}}^{\text{eff}}\} = \{0.034, 0.903 \text{ eV}\}$ .

	Model	$10^5 \omega_b$	$10^3 \omega_{\text{cdm}}$	$H_0$	$\ln(10^{10} A_s)$	$n_s$	$\tau_{\text{reio}}$	$\Delta N_{\text{eff}}$	$M_{\text{sp}}^{\text{eff}}$ [eV]
Set I	NT	2.85	1.26	0.263	0.010	0.0019	0.0059	0.0038	0.080
	DW	2.85	1.11	0.268	0.010	0.0020	0.0059	0.0034	0.076
Set II	NT	3.54	1.01	0.273	0.013	0.0025	0.0067	0.029	0.027
	DW	3.68	0.96	0.278	0.012	0.0024	0.0067	0.028	0.029

Table IV: Comparison of the projected  $1\sigma$  errors from CMB-S4 for parameters  $\theta_i$ , marginalized over all other parameters for the NT and DW models.

for the NT model. More  $\Delta N_{\text{eff}}$  leads to more damping of the primary CMB spectra at higher  $\ell$ . Although the free-streaming velocity of the LiMR is more in the case of set II, the suppression of the lensing spectrum  $C_\ell^{\phi\phi}$  is less compared to set I. This is because, in set I, the CDM component is reduced at the cost of the LiMR component. The net effect is less clustering power and hence greater suppression of  $C_\ell^{\phi\phi}$ . For set II, structure grows more efficiently, despite the fact that  $\langle v_{\text{fs}} \rangle$  is ten times greater than that for set I, leading to stronger lensing potentials and hence  $C_\ell^{\phi\phi}$  is less suppressed. We will restrict our analyses to the linear regime since non-linear matter power spectrum corrections (via HALOFIT or HMcode) are not appropriate for models where the dark sector includes massive hot dark matter or warm dark matter components.

Before analysing these two sets, as a preliminary study, we will compare the two non-thermal models, with the LiMR masses fixed to zero, with the  $\Lambda$ CDM model extended by the  $N_{\text{eff}}$  parameter, which we will refer to as the  $\nu\Lambda$ CDM model. We will perform the Fisher analysis by marginalizing over the six  $\Lambda$ CDM parameters, along with  $N_{\text{eff}}$  for the  $\nu\Lambda$ CDM model, or  $B_{\text{sp}}$  for the NT model, or  $\chi$  for the DW model, in order to find the constraints on  $N_{\text{eff}}$  around  $\Delta N_{\text{eff}} = 0$ . To this end, we use the following fiducial values for the seventh parameter:  $N_{\text{eff}} = 0$ ,  $B_{\text{sp}} = 0$ , and  $\chi = 0$  for the  $\nu\Lambda$ CDM model, the NT model, and the DW model, respectively<sup>7</sup>. We use the following fiducial values for the  $\Lambda$ CDM model parameters [5]:  $\omega_b = 0.02224$ ,  $\omega_{\text{cdm}} = 0.1179$ ,  $h = 0.663$ ,  $A_s = 2.082 \times 10^{-9}$ ,  $n_s = 0.9589$ , and  $\tau_{\text{reio}} = 0.05$ . The  $1\sigma$  projected uncertainties on  $N_{\text{eff}}$  from CMB-S4 were found to

be as follows:

$$\sigma(N_{\text{eff}}) = \begin{cases} 0.028 & (\nu\Lambda\text{CDM}) \\ 0.025 & (\text{NT}) \\ 0.029 & (\text{DW}) \end{cases} \quad (25)$$

The fact that we obtain similar constraints for these three models (when expanding around the same fiducial cosmology) is consistent with the expectation that these models would be indistinguishable since they have the same phenomenological parameters  $\Delta N_{\text{eff}} \approx 0$  and  $M_{\text{sp}}^{\text{eff}} = 0 \text{ eV}$ .

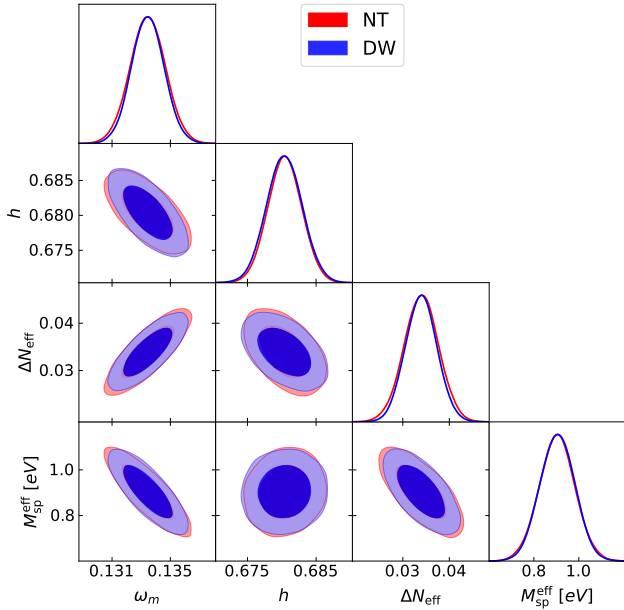
#### A. Forecasts for inflaton-decay non-thermal and Dodelson-Widrow models

Now we move on to the results of the Fisher forecasts for the LiMRs with the fiducial values in Table II.

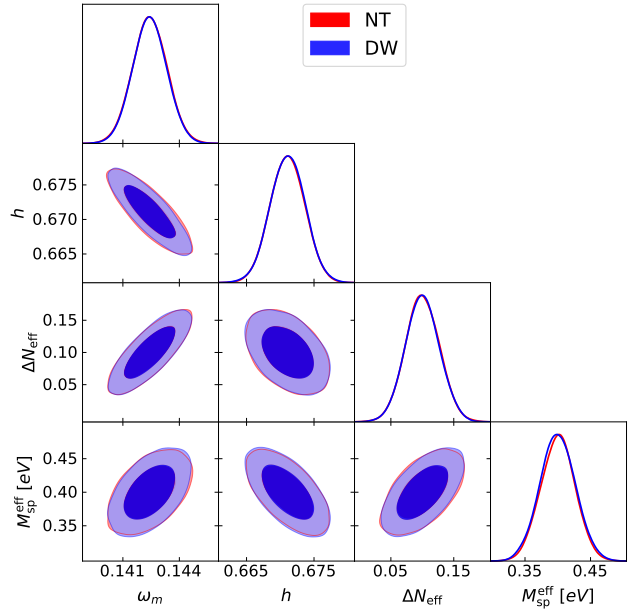
- Set I: The projected  $1\sigma$  uncertainties on the fiducial model parameters are reported in Table III. The Fisher ellipses for the parameters  $\{\omega_m = \omega_b + \omega_{\text{cdm}}, h, \Delta N_{\text{eff}}, M_{\text{sp}}^{\text{eff}}\}$  are shown in Fig. 4a. As expected, combined analysis of Planck and CMB-S4 leads to tighter constraints on the parameters. From Table IV, one can see that the NT model and the DW model uncertainties are in close agreement with each other. Of our particular interest are the phenomenological parameters, whose  $1\sigma$  uncertainties from CMB-S4+Planck are

$$1\sigma(\Delta N_{\text{eff}}) = \begin{cases} 0.0037 & (\text{NT}) \\ 0.0033 & (\text{DW}) \end{cases}, \quad (26)$$

<sup>7</sup> For the numerical implementation, we set  $B_{\text{sp}} = 10^{-6}$  and  $\chi = 2.92 \times 10^{-6}$ .



(a) Fisher plots for the NT and DW models with fiducial values set I.



(b) Same as (a) with fiducial values set II.

Figure 4: The posterior distributions and Fisher ellipses for the parameters  $\{\omega_m = \omega_b + \omega_{\text{cdm}}, h, \Delta N_{\text{eff}}, M_{\text{sp}}^{\text{eff}}\}$  (plotted using `getdist`).

and

$$1\sigma(M_{\text{sp}}^{\text{eff}}) = \begin{cases} 80 \text{ meV} & (\text{NT}) \\ 76 \text{ meV} & (\text{DW}) \end{cases} . \quad (27)$$

- Set II: The Fisher plots are shown in Fig. 4b and the  $1\sigma$  uncertainties are given in Table IV. We again see that the DW model parameter uncertainties agree quite well with the corresponding uncertainties for the NT model. With this set of fiducial values, we obtain the following  $1\sigma$  uncertainties from CMB-S4+Planck:

$$1\sigma(\Delta N_{\text{eff}}) = \begin{cases} 0.028 & (\text{NT}) \\ 0.027 & (\text{DW}) \end{cases} , \quad (28)$$

and

$$1\sigma(M_{\text{sp}}^{\text{eff}}) = \begin{cases} 26 \text{ meV} & (\text{NT}) \\ 27 \text{ meV} & (\text{DW}) \end{cases} . \quad (29)$$

We see that the relative uncertainties on  $M_{\text{sp}}^{\text{eff}}$  are 8.9%(8.4%) and 6.5%(6.75%), whereas the relative uncertainties on  $\Delta N_{\text{eff}}$  are 10.9%(9.7%) and 28%(27%), for the NT(DW) model. So the relative uncertainties on  $M_{\text{sp}}^{\text{eff}}$  slightly worsen while there is a significant improvement in the relative uncertainties on  $\Delta N_{\text{eff}}$  in going from set II to set I. In Fig. 5 we compare the Fisher ellipses and the posteriors for the two sets.

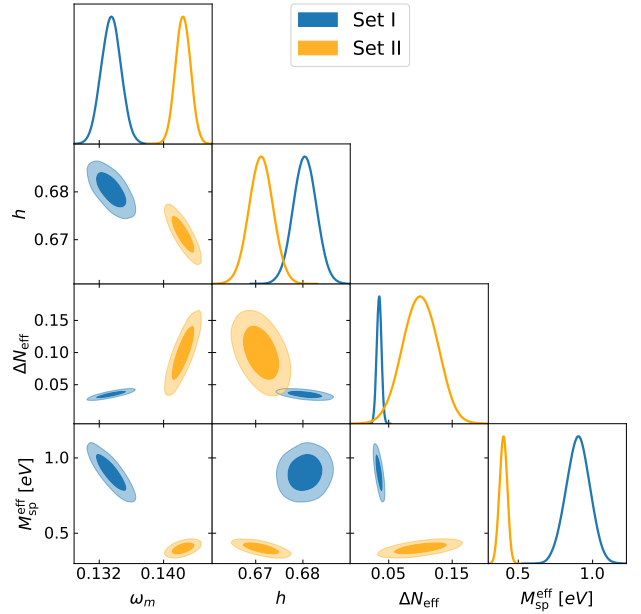


Figure 5: Comparative Fisher plots for the two sets of fiducial values considered in the text.

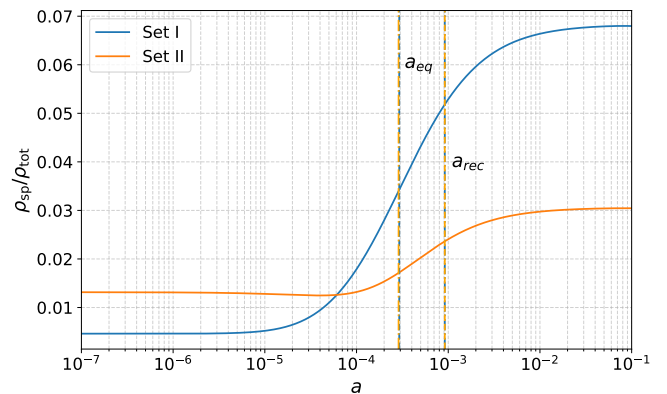
## B. Discussion

Our results reveal the following noteworthy features pertaining to the phenomenological parameters.

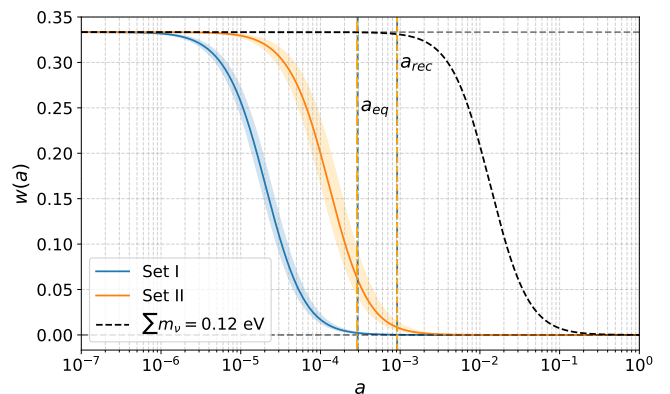
- (i) There is significant difference in the relative uncertainties on  $\Delta N_{\text{eff}}$  for the two sets analyzed (as seen in equations Eq. (26) and Eq. (28)).
- (ii) The phenomenological parameters,  $\Delta N_{\text{eff}}$  and  $M_{\text{sp}}^{\text{eff}}$ , are negatively correlated for the heavier particle but positively correlated for the lighter one.
- (iii)  $\Delta N_{\text{eff}}$  and  $h$  are negatively correlated for both data sets. Note that this is contrary to what happens for standard (massless) neutrinos –  $h$  and  $N_{\text{eff}}$  are positively correlated.

In this section, we will discuss these features and provide explanations for them.

First, let us look at bullet point (i). We will argue that the large difference in  $\Delta N_{\text{eff}}$  constraints when considering the two sets of fiducial parameter values within the same model arises from the LiMR’s contribution to the energy budget just prior to recombination, in particular their relative contributions to the “matter” (with energy density scaling as  $a^{-3}$ ) and “radiation” (energy density scaling as  $a^{-4}$ ) components. The heavier particle (set I), owing to its lower number density, has a relatively lesser contribution to the relativistic energy density, compared to the lighter particle (set II), but it contributes significantly more to the matter density, as demonstrated in Fig. 6a. Evolution of the effective equation of state parameter of the LiMRs are plotted in Fig. 6b. The heavier particle becomes non-relativistic just before matter-radiation equality. By recombination, it therefore contributes solely to the total matter density. Contrast this with the lighter particle of set II (contributing more to  $N_{\text{eff}}$ ), which is caught in transition at matter-radiation equality and becomes completely non-relativistic only after recombination. As such, the CMB becomes sensitive to the heavier relic almost exclusively through its effect on the weak lensing signal. When the lensing signal was excluded from the Fisher computations, we obtained  $\sigma(\Delta N_{\text{eff}}) \sim 0.01$  (0.04) for the heavier (lighter) particle. Even in the absence of lensing, the tighter constraint for set I is due to the fact that the particle contributes solely as extra matter by recombination. Any shift in the total matter density at that epoch alters the acoustic peak structure in a way that  $\Delta N_{\text{eff}}$  (being zero at recombination) cannot mimic. Since  $\Delta N_{\text{eff}}$  has no freedom to absorb these matter-like changes, the primary spectra pin down its fiducial value to a higher precision. The effect of lensing information is more pronounced in the case of set I (as mentioned above) which leads to a greater improvement in the uncertainty on  $\Delta N_{\text{eff}}$  (by a factor of  $\sim 3$ ) as compared to set II (where there is a  $\sim 30\%$  improvement). The heavier LiMR is more degenerate with  $\omega_m$  at recombination compared to the lighter one – for a given



(a) Evolution of the energy density  $\rho_{\text{sp}}$  of the particle, as a fraction of the total energy density  $\rho_{\text{tot}}$  of the Universe, with the scale factor.



(b)  $w$  vs  $a$  plot for the LiMRs corresponding to the two sets of fiducial values. For reference, we have also shown the behavior of massive standard (degenerate) neutrinos with  $\sum m_\nu = 0.12$  eV. The shaded regions correspond to the  $1\sigma$  uncertainties on  $w$ .

Figure 6: Comparison of the evolution of the equation of state parameter and the energy density of the LiMR for the two sets of fiducial values (for the NT model).

total matter content (baryons+CDM+LiMR), replacing a fraction of  $\omega_m$  with  $\omega_{\text{sp}}$  has negligible impact for the heavier particle – this explains the slightly degraded relative uncertainty on  $M_{\text{sp}}^{\text{eff}}$  for set I as compared to set II.

Now we move on to bullet point (ii) – the correlation between the phenomenological parameters. For the heavier particle, an increase in  $\omega_m$  causes a disproportionate decrease in the angular diameter distance at recombination  $d_{A*}$  compared to the sound horizon at recombination  $r_{s*}$ ,  $\Delta N_{\text{eff}}$  increases so as to keep  $\theta_* = r_{s*}/d_{A*}$  unchanged.<sup>8</sup> Recall that the scale factor at matter

<sup>8</sup> Observations put tight constraints on  $\theta_*$ , its value is essentially fixed [5].

radiation equality,  $a_{\text{eq}}$  is tightly constrained by observations. Since the heavier particle contributes solely as matter at matter-radiation equality,  $M_{\text{sp}}^{\text{eff}}$  has to decrease with increasing  $\omega_m$ , since  $1 + z_{\text{eq}} = \omega_r/(\omega_m + \omega_{\text{sp}})$ . So with increasing  $\omega_m$ ,  $\Delta N_{\text{eff}}$  has to increase and  $M_{\text{sp}}^{\text{eff}}$  has to decrease. This explains the negative correlation between  $\Delta N_{\text{eff}}$  and  $M_{\text{sp}}^{\text{eff}}$  for the heavier particle. For the lighter particle, the relation between  $\Delta N_{\text{eff}}$  and  $M_{\text{sp}}^{\text{eff}}$  is more direct. There is a non-zero contribution to  $\Delta N_{\text{eff}}$  during recombination (this is not so for the heavy particle case). Therefore, decreasing  $M_{\text{sp}}^{\text{eff}}$  also implies that the LiMR contributes less to the relativistic energy density during recombination (due to decreased number density of the particles). Hence the positive correlation between  $M_{\text{sp}}^{\text{eff}}$  and  $\Delta N_{\text{eff}}$ . Note that the change in the sign of correlation between  $M_{\text{sp}}^{\text{eff}}$  and  $\omega_m$  (flips from negative to positive) is due to the inclusion of the lensing effects, i.e., not influenced by pre-recombination era physics. More  $\omega_m$  enhances lensing strength, compensating for the suppression due to the relic's free streaming.

Finally, let us look at (iii) — the negative correlation between  $\Delta N_{\text{eff}}$  and  $h$ . Let us recapitulate the story in the case of standard neutrinos. For standard neutrinos,  $h$  and  $N_{\text{eff}}$  are positively correlated. This is because increasing  $N_{\text{eff}}$  increases the Hubble parameter at recombination  $H_*$ , thereby decreasing  $r_{s*}$  (without much impact on  $d_{A*}$ ), and  $h$  increases (decreasing  $d_{A*}$ ) to keep the acoustic scale at recombination  $\theta_* = r_{s*}/d_{A*}$  fixed. In our case this correlation flips sign, for the following reason. We are introducing a massive particle which behaves more like matter than radiation during recombination. Changing  $\Delta N_{\text{eff}}$  not only has a lesser impact on  $H_*$  compared to the massless case, but it also has a significantly greater impact on  $d_{A*}$ . So increasing  $\Delta N_{\text{eff}}$  reduces  $d_{A*}$  more than  $r_{s*}$  and hence  $h$  decreases to keep  $\theta_*$  fixed.

Of course, all these explanations have a qualitative element to them, the exact quantitative nature of the correlations are as obtained by our numerics.

## V. HIGHER MOMENTS

So far we discussed the impact of LiMRs in terms of two phenomenological parameters  $M_{\text{sp}}^{\text{eff}}$  and  $\Delta N_{\text{eff}}$  which are proportional to the zeroth and first moments of the phase space distribution function respectively. We obtained similar results for both the inflaton-decay model and the Dodelson-Widrow model once  $M_{\text{sp}}^{\text{eff}}$  and  $\Delta N_{\text{eff}}$  are matched, inspite of the noticeably different forms of the distribution functions (see Fig. 1). Ref. [43] claimed that different models with the same  $M_{\text{sp}}^{\text{eff}}$  and  $\Delta N_{\text{eff}}$  would be difficult to distinguish, especially using observables at the linear perturbation theory level. To check how well this claim holds up at the noise levels expected at the CMB-S4 experiment, we consider two distribution functions with matched zeroth and first moments — the Dodelson-Widrow distribution  $\hat{f}_{DW}(q)$  and another distribution  $\hat{f}(q)$  which starts differing from the

Dodelson-Widrow distribution at the level of the second moment. In order to include the effect of the second moment we consider an Edgeworth-like expansion about the Dodelson-Widrow distribution, which constitutes a continuous deformation of the Dodelson-Widrow distribution:

$$\hat{f}(q) = \hat{f}_{DW}(q) [\alpha_0 P_0(q) + \alpha_1 P_1(q) + \alpha_2 P_2(q)], \quad (30)$$

where  $\hat{f}_{DW}(q) = \chi[\exp(q) + 1]^{-1}$ . The functions  $P_m(q)$  are  $m$ -th order polynomials in  $q$ , orthonormal with respect to the measure  $q^2/(e^q + 1)$  [36],

$$\int_0^\infty dq \frac{q^2}{e^q + 1} P_m(q) P_n(q) = \delta_{mn}. \quad (31)$$

The modified distribution function in (30) can be rewritten as

$$\hat{f}(q) = \frac{\chi}{e^q + 1} [\alpha + \beta q + \gamma q^2], \quad (32)$$

where  $\alpha, \beta$ , and  $\gamma$  are dimensionless constants, and its  $n$ -th moment computed as

$$Q^{(n)} = \int_0^\infty dq q^{2+n} \hat{f}(q). \quad (33)$$

Setting  $Q^{(0)} = Q_{DW}^{(0)}$  and  $Q^{(1)} = Q_{DW}^{(1)}$ , i.e., matching the first two moments, we can solve for  $\alpha$  and  $\beta$  in terms of  $\gamma$  to obtain

$$\hat{f}(q) = \frac{\chi}{e^q + 1} [1 + 13.0551\gamma - 8.24864\gamma q + \gamma q^2], \quad (34)$$

where  $\gamma$  is now a free parameter which determines how much  $\hat{f}(q)$  deviates from  $\hat{f}_{DW}(q)$ . However, to be a valid distribution function,  $\hat{f}(q)$  has to be non-negative everywhere. This requirement limits the value of  $\gamma$  to the range  $0 \leq \gamma \leq 0.25$ , where  $\gamma = 0$  corresponds to the DW distribution (see Fig. 7). That  $\hat{f}(q)$  goes to zero at large  $q$  values is ensured by the  $1/(e^q + 1)$  factor which goes like  $e^{-q}$  for large  $q$ . The projected  $1\sigma$  uncertainties on all the parameters, obtained from our Fisher analysis with the fiducial values set I, for the cases  $\gamma = 0$  and  $\gamma = 0.25$  are given in Table V. The corresponding Fisher ellipses and posterior distributions for the phenomenological parameters are shown in Fig. 8.

To determine whether the CMB-S4 experiment will be able to distinguish between these two models, we performed Fisher forecasts by marginalizing over the six  $\Lambda$ CDM parameters, the two phenomenological parameters  $\Delta N_{\text{eff}}$  and  $M_{\text{sp}}^{\text{eff}}$ , along with the  $\gamma$  parameter. In this case, we obtained the following projected uncertainties on  $\Delta N_{\text{eff}}$ ,  $M_{\text{sp}}^{\text{eff}}$ , and  $\gamma$ :

1. For  $\gamma = 0$ , we get  $\sigma(\Delta N_{\text{eff}}) = \pm 0.0046$ ,  $\sigma(M_{\text{sp}}^{\text{eff}}) = \pm 0.097$ , and  $\sigma(\gamma) = +0.178$ .
2. For  $\gamma = 0.25$ , we get  $\sigma(\Delta N_{\text{eff}}) = \pm 0.0039$ ,  $\sigma(M_{\text{sp}}^{\text{eff}}) = \pm 0.129$  eV, and  $\sigma(\gamma) = -0.163$ .

Parameter	$10^5 \omega_b$	$10^3 \omega_{\text{cdm}}$	$H_0$	$\ln(10^{10} A_s)$	$n_s$	$\tau_{\text{reio}}$	$\Delta N_{\text{eff}}$	$M_{\text{sp}}^{\text{eff}}$ [eV]
$1\sigma$ error ( $\gamma = 0$ )	2.77	1.11	0.25	0.0099	0.0019	0.0056	0.0033	0.076
$1\sigma$ error ( $\gamma = 0.25$ )	2.77	1.39	0.22	0.0095	0.0018	0.0054	0.0033	0.111

Table V: Projected uncertainties on the parameters from Planck+CMB-S4 for the modified DW distribution with fiducial values set I.

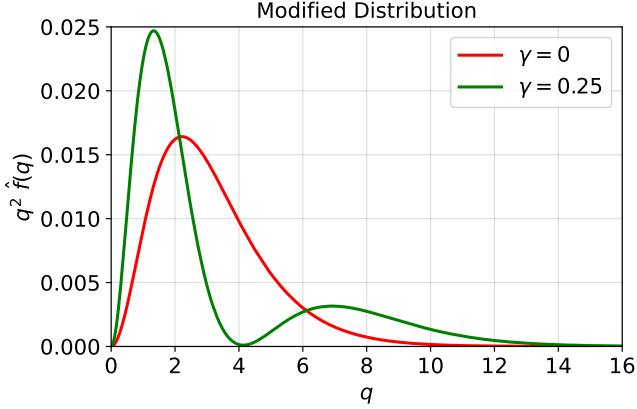


Figure 7: Plot showing the modified distribution function for  $\gamma = 0$  (same as DW) and  $\gamma = 0.25$ , with the momentum expressed in terms of the neutrino temperature today.

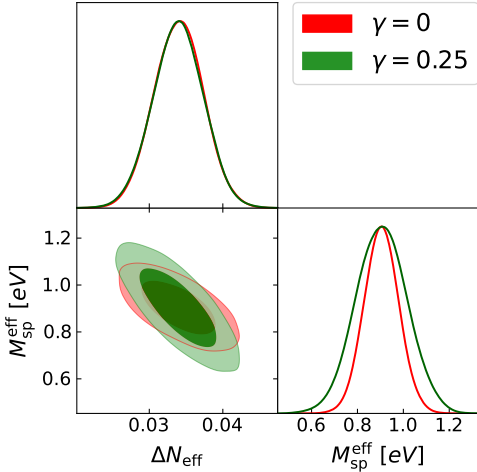


Figure 8: Fisher plots of the phenomenological parameters for the modified DW distribution.

So for  $\gamma = 0$ , the modified distribution with  $\gamma = 0.25$  is  $\sim 1.4\sigma$  away, and for  $\gamma = 0.25$ , the DW distribution ( $\gamma = 0$ ) is  $\sim 1.5\sigma$  away, when we consider the posterior probability distribution of the  $\gamma$  parameter. This indicates that it is unlikely that CMB-S4 would be able to distinguish between the two distributions at a statistical significance. We believe this generalizes to any

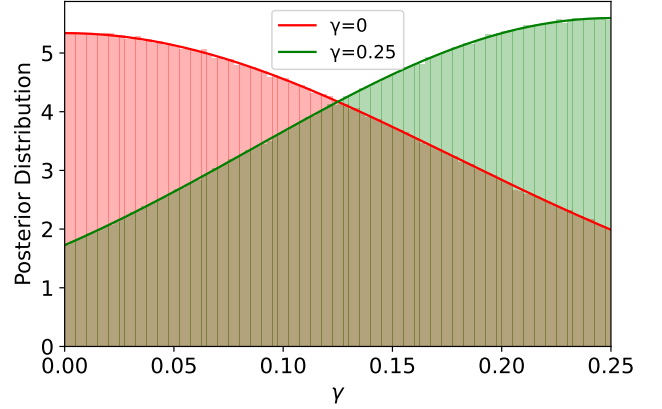


Figure 9: Comparison of the posterior distributions of the parameter  $\gamma$  for the modified DW distribution. The significant overlap ( $\sim 60\%$ ) indicates that it is unlikely that CMB-S4 would be able to distinguish between the two.

two LiMR models having the same values of  $\Delta N_{\text{eff}}$  and  $M_{\text{sp}}^{\text{eff}}$  irrespective of how much the higher moments differ. However, for the CV limited experiment, the two models were found to be distinguishable. When assuming the  $\gamma = 0$  case to be the true model, we found the model corresponding to the  $\gamma = 0.25$  case to lie outside the  $\sim 5.7\sigma$  C.L., whereas when considering the latter model to be the true one, the former was found to lie outside the  $\sim 3.6\sigma$  C.L. So a future experiment with lower noise levels (i.e., better sensitivity) than the CMB-S4 experiment, for instance the CMB-HD experiment [54], can potentially differentiate between two models with the same first two moments.

Note that the uncertainties on  $\gamma$  has been obtained using Eq. (14), and we have not implemented the hard prior on  $\gamma$ , i.e.,  $0 \leq \gamma \leq 0.25$ . Fig. 9 shows the truncated posterior distributions. We quantify the distinguishability between the two cases by computing the overlap fraction. The analysis reveals a  $\sim 60\%$  probability mass overlap reaffirming that CMB-S4 data would not be able to distinguish between these models. In order to incorporate the valid range of  $\gamma$  in our Fisher analysis, we computed the covariance matrix by numerically sampling a multivariate Gaussian from the inverse of the Fisher matrix and rejecting those realizations for which  $\gamma$  lies outside the allowed range. We obtained the following median values and asymmetric uncertainties (due to the non-

Gaussian nature of the posterior distribution induced by the hard prior; see footnote 2):

$$\gamma = 0.098_{-0.098}^{+0.088} \quad \text{and} \quad \gamma = 0.156_{-0.087}^{+0.065}, \quad (35)$$

corresponding to the fiducial values  $\gamma = 0$  and  $\gamma = 0.25$  respectively. Even with the imposition of the hard priors, which leads to tighter (asymmetric) constraints, the distribution with  $\gamma = 0.25$  is within the  $3\sigma$  uncertainty threshold of the  $\gamma = 0$  distribution and vice versa. This shows that including the hard prior does not change our conclusion above and moving on we shall use the symmetric uncertainties on  $\gamma$  obtained previously.

The physical quantity related to the second moment of the LiMR distribution function is the "pressure" of the LiMRs. We define the quantity  $f_P$ , the *fractional pressure* of the LiMRs, as ( $g_s''$  is a degeneracy factor)

$$f_P \equiv \frac{P_{\text{sp}}}{P_\nu} = \frac{g_s''}{15/16} \underbrace{\left[ \int dp p^4 \hat{f}(p) \right]}_{Q^{(2)}} / \left[ \frac{45\zeta(5)}{2} (T_\nu^{\text{id}})^5 \right]. \quad (36)$$

While the fiducial values of all the  $\Lambda$ CDM parameters as well as that of  $\Delta N_{\text{eff}}$  and  $M_{\text{sp}}^{\text{eff}}$  are the same, the fiducial values of  $f_P$  differ between the cases  $\gamma = 0$  and  $\gamma = 0.25$ . This is a consequence of differing second moments as mentioned above. The fiducial values of  $f_P$  are

$$f_P = \begin{cases} 0.180 & (\gamma = 0) \\ 0.265 & (\gamma = 0.25) \end{cases} \quad (37)$$

The uncertainties on  $\gamma$  can be translated to the uncertainties on the second moment by using  $Q^{(2)} = Q_{DW}^{(2)} (= 0.79325) + 1.4865\gamma$ . Hence the projected uncertainties on  $f_P$  are

$$\sigma(f_P) = +0.240 \quad \text{and} \quad \sigma(f_P) = -0.286 \quad (38)$$

for the cases  $\gamma = 0$  and  $\gamma = 0.25$  respectively. In Fig. 10, we plot the equation of state parameter  $w$  as a function of the scale factor for the modified distribution, for  $\chi = 0.034$  and  $m_{\text{sp}} = 26.43$  eV, with  $\gamma = 0$  and  $\gamma = 0.25$ . The difference between the two curves arises from the difference in the pressures, or equivalently  $f_P$ , and not from  $\rho_{\text{sp}}$ , which is the same for both cases. The inset plot zooms in on a region of the curves and shows the  $1\sigma$  uncertainties on  $w$ , derived from the uncertainties on  $\gamma$ . The overlap between the pink and green shaded regions again indicates that CMB-S4 data would not be able to rule out one model in favor of the other.

If we include a  $\delta y^3$  term in the expansion (32) and match the first three moments, we find that the new parameter  $\delta$  can lie in the range  $[0, 0.015]$ , where the upper bound is an order of magnitude lesser than the previous case. This suggests that matching the first three moments essentially fixes the form of the modified distribution function with little room for deviation from the

DW case. Similar to Fig. 10, in Fig. 11, we plot the evolution of the equation of state parameter  $w$  as a function of the scale factor  $a$  for the new modified distribution with  $\delta = 0$  and  $\delta = 0.015$ . We find that the curves corresponding to  $\delta = 0$  and  $\delta = 0.015$  overlap. Thus we conclude that no future CMB experiment would be able to distinguish between two LiMR models which agree on the first three moments of the corresponding LiMR distribution functions. This is likely to generalize to the case of matching even higher moments. Note that this conclusion may not extend to non-linear scales, a matter that is currently under investigation.

## VI. CONCLUSION

The presence of LiMRs affects the evolution of the Universe. When relativistic, they behave as dark radiation and contribute to the relativistic energy density of the Universe, whereas when non-relativistic, they behave as dark matter. The upcoming CMB-S4 experiment is expected to measure various cosmological parameters with unprecedented precision. In the context of light relics,  $N_{\text{eff}}$  is an important parameter. If the measured value of  $N_{\text{eff}}$  exceeds the SM prediction of 3.044, it would indicate the presence of dark sector light relics (or the need to modify the thermal history of the Universe). Conservative configurations of the CMB-S4 experiment can reach  $\sigma(N_{\text{eff}}) \sim 0.02-0.03$  [12]. For LiMRs, another important parameter is the relic mass, or rather its contribution to the non-relativistic energy density of the Universe today, captured by the parameter  $M_{\text{sp}}^{\text{eff}}$ . Another important aspect of particles contributing to  $N_{\text{eff}}$  is their momentum distribution which is often tied to interesting aspects of the physics of the early Universe and particle physics such as production mechanism and interaction rates. Therefore, extracting the relation between distribution functions and observables is an important question.

In this work, we performed Fisher analyses to check how much CMB-S4 data would be able to constrain these parameters for *non-thermal* LiMR models. We primarily concerned ourselves with a model of inflaton/moduli decay giving rise to LiMRs of mass  $m_{\text{sp}}$ , with a branching ratio  $B_{\text{sp}}$ . The LiMRs so produced follow a non-thermal distribution, unlike thermalized LiMRs which follow Fermi-Dirac or Bose-Einstein distribution, depending on the statistics [32, 55]. We also considered the Dodelson-Widrow distribution throughout. The main conclusions of our work are as follows:

- We obtained tighter constraint on  $\Delta N_{\text{eff}}$  ( $\sim 10^{-3}$ ) for a LiMR which becomes non-relativistic well before recombination, around the epoch of matter-radiation equality. However, the constraint so obtained might be misleading owing to the fact that the LiMR does not contribute to  $\Delta N_{\text{eff}}$  at recombination, which is a measure for additional "relativistic" degrees of freedom. The tighter constraint (further enhanced by lensing) is owing to the fact that

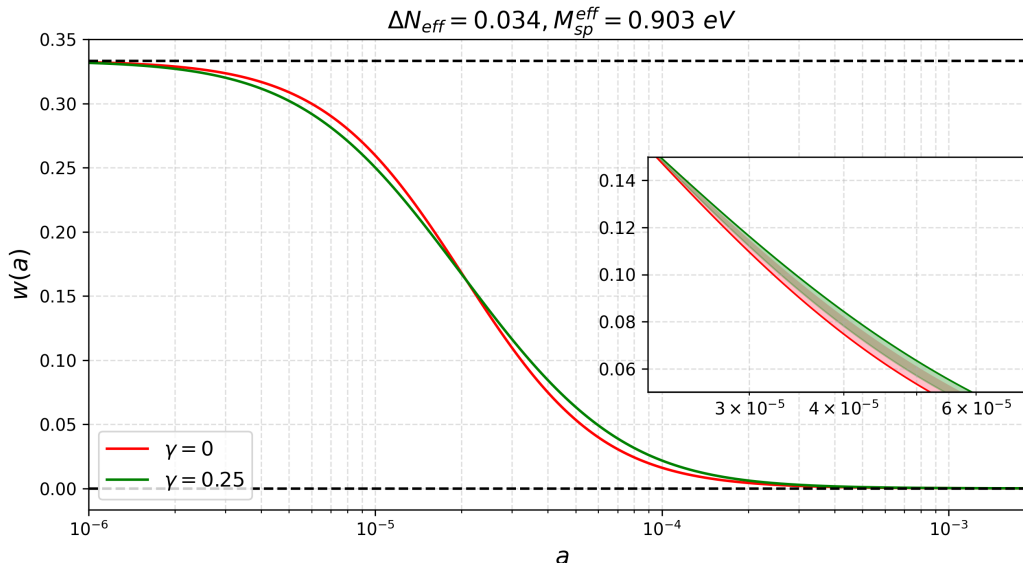


Figure 10:  $w$  vs  $a$  plot for the modified distribution (34) with  $\gamma = 0$  (DW) and  $\gamma = 0.25$ . Shaded regions in the inset corresponds to the one-sided uncertainties on  $w$  derived from the uncertainties on  $\gamma$ .

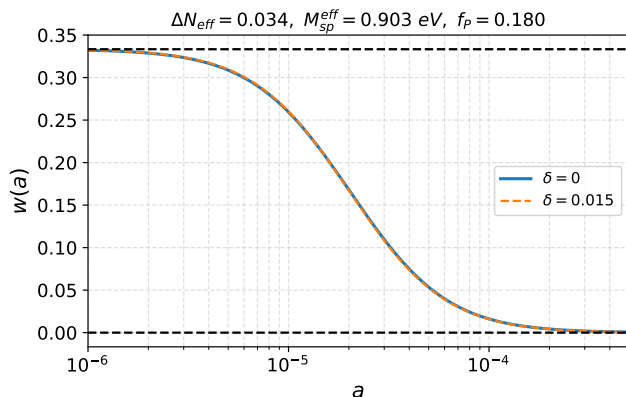


Figure 11: Evolution of  $w$  with  $a$  for the DW and the modified distribution when the first three moments are matched and the fourth moment is made to differ by the maximum possible extent. The exact overlap between the curves indicates the indistinguishability of the two models.

changes in  $\omega_m (= \omega_b + \omega_{\text{cdm}})$  or  $\omega_{\text{sp}}$  cannot be replicated by changes in  $\Delta N_{\text{eff}}$  which is zero by recombination. For a LiMR which transitions in the matter dominated era and becomes completely non-relativistic just after recombination, we obtained a weaker constraint on  $\Delta N_{\text{eff}}$  ( $\sim 10^{-2}$ ) in line with the expected uncertainty for light relics [12].

- Our analysis in section IV B (see Fig. 4) also revealed interesting correlations between model parameters and observables. In particular, we

obtained negative correlation between the phenomenological parameters for set I but positive correlation for set II. These can be relevant in endeavors to connect cosmology with particle physics model building.

- We compared our results for the non-thermal model with those of the Dodelson-Widrow model, and found that CMB-S4 data would yield similar constraints on the parameters for these models once the phenomenological parameters  $\Delta N_{\text{eff}}$  and  $M_{\text{sp}}^{\text{eff}}$  (related to the first two moments of the distribution function) are matched.
- We also compared the Dodelson-Widrow distribution with a modified distribution (which can be considered as a perturbed Dodelson-Widrow distribution), artificially constructed so as to match the first two moments but differing to the maximum possible extent in the higher moments. We deduced that CMB-S4 data would be unable to tell even these two distributions apart. We believe this generalizes to any two distribution functions with matching first two moments.

LiMRs not only affect the CMB primary and lensing power spectra but also affect the matter power spectrum due to their free streaming/clustering effects. In fact, the effects on the matter power spectrum feed back to the CMB lensing power spectrum. As such, future galaxy surveys such as LSST and Euclid (VRO) can also probe the impact of LiMRs, and one can perform Fisher analyses for such galaxy surveys. Combining CMB and LSS information is crucial for obtaining optimal constraints on LiMRs, particularly for those relics which

are not fully relativistic at recombination, as has been observed in Ref. [32], for example. This we keep for future work. Moreover, going beyond linear theory to the non-linear matter power spectrum unlocks new information about LiMRs — chiefly through the distinctive, scale-dependent damping they induce, which cannot be mimicked by simply retuning the  $\Lambda$ CDM parameters [56]. This indicates that degeneracies that exist on large (linear) scales can be broken by using signatures on small (non-linear) scales. In Ref. [56], the authors also found that non-linear effects can reveal differences between LiMR models that appear identical at the linear level. Remarkably, these distinctions arise from differences in the momentum distribution functions of LiMRs. Since these distributions are intimately connected to the production mechanisms of non-thermal relics, the resulting non-linear signatures could provide valuable insight into early Universe physics—insight that linear analyses, including the present study, are inherently insensitive to.

## ACKNOWLEDGMENTS

RKS thanks the Alexander von Humboldt Foundation for their support. AB acknowledges support from the Science and Engineering Research Board (SERB) India via the Startup Research Grant SRG/2023/000378.

## Appendix A: INFLATON/MODULI DECAY MODEL

In this appendix, we discuss briefly the production mechanism leading to the form of the non-thermal distribution function (4) for the LiMRs. Further details can be found in Ref. [40]. We start with a matter-dominated Universe at a (dimensionless) ‘initial time’ ( $\theta \equiv t/\tau = 0$ ) and evolve the Universe using the following equations up to a time  $\theta^*$  which is large enough to ensure that almost all the  $\phi$  particles have decayed<sup>9</sup>:

$$\dot{\rho}_m + 3H\rho_m = -\frac{\rho_m}{\tau}, \quad (\text{A1})$$

$$\dot{\rho}_r + 4H\rho_r = +\frac{\rho_m}{\tau}, \quad (\text{A2})$$

and

$$H = \frac{\dot{a}}{a} = \sqrt{\frac{\rho_m + \rho_r}{3M_{\text{pl}}^2}}, \quad (\text{A3})$$

where  $\rho_m = \rho_\phi$  denotes the energy density in matter and  $\rho_r = \rho_{\text{sp}} + \rho_{\text{SM}}$  is the energy density in radiation. As a

<sup>9</sup> We choose  $\theta^* = 15$  in practice.

result of decays, the comoving inflaton/modulus number density falls off as  $N(t) = N(0)e^{-t/\tau}$  where

$$N(0) \equiv \frac{\rho_m(0)}{m_\phi} = \frac{4\alpha M_{\text{pl}}^2}{3\tau^2 m_\phi} \quad (\alpha \gg 1). \quad (\text{A4})$$

Combining this with the fact that the energy of a particle produced at  $t = t_d$  will evolve according to (with  $\hat{E} = E(t_d)$ )

$$E(t) = \hat{E} \left( \frac{a(t_d)}{a(t)} \right) = \frac{m_\phi}{2} \left( \frac{a(t_d)}{a(t)} \right), \quad (\text{A5})$$

one can get the physical number density spectrum of the particles,

$$\begin{aligned} dN_t &= \frac{1}{a^3(t)} \frac{2B_{\text{sp}}}{\tau} N(0) e^{-t_d/\tau} dt_d \\ &= \frac{2B_{\text{sp}}}{\hat{s}^3(\theta)\tau} N(0) e^{-\hat{s}^{-1}(y)} \frac{dE}{E\hat{H}(\hat{s}^{-1}(y))}. \end{aligned} \quad (\text{A6})$$

One hence arrives at the following late-time momentum distribution function by red-shifting the energy of the particles from their time of production

$$f(\mathbf{q}) = \frac{32}{\pi \hat{E}^3} \left( \frac{N(0)B_{\text{sp}}}{\hat{s}^3(\theta^*)} \right) \frac{\exp(-\hat{s}^{-1}(y))}{|\mathbf{q}|^3 \hat{H}(\hat{s}^{-1}(y))}, \quad (\text{A7})$$

where  $y = (|\mathbf{q}|/4)\hat{s}(\theta^*)$  and  $|\mathbf{q}|$  is constrained so that

$$\frac{4}{\hat{s}(\theta^*)} < |\mathbf{q}| < 4. \quad (\text{A8})$$

The argument of the distribution function is  $|\mathbf{q}| \equiv |\mathbf{p}|/T_{\text{ncdm},0}$  where

$$T_{\text{ncdm},0} = 0.418 \left( \frac{m_\phi^2 \tau}{M_{\text{pl}}} \right)^{1/2} \frac{T_{\text{cmb}}}{(1 - B_{\text{sp}})^{1/4}} \equiv \zeta T_{\text{cmb}} \quad (\text{A9})$$

is the temperature of the non-cold-dark matter species today, expressed in terms of the CMB temperature.

## Appendix B: NUMERICAL DERIVATIVES

The numerical differentiation was done using the three-point central difference formula with equal left and right step sizes (for two-sided derivatives)

$$\frac{\partial C_\ell(\theta_0)}{\partial \theta} = \frac{C_\ell(\theta_0 + \Delta s) - C_\ell(\theta_0 - \Delta s)}{2\Delta s}, \quad (\text{B1})$$

or the two-point forward/backward difference formula (for one-sided derivatives)

$$\begin{aligned} \left. \frac{\partial C_\ell(\theta_0)}{\partial \theta} \right|_+ &= \frac{C_\ell(\theta_0 + \Delta s) - C_\ell(\theta_0)}{\Delta s}, \\ \left. \frac{\partial C_\ell(\theta_0)}{\partial \theta} \right|_- &= \frac{C_\ell(\theta_0) - C_\ell(\theta_0 - \Delta s)}{\Delta s}. \end{aligned} \quad (\text{B2})$$

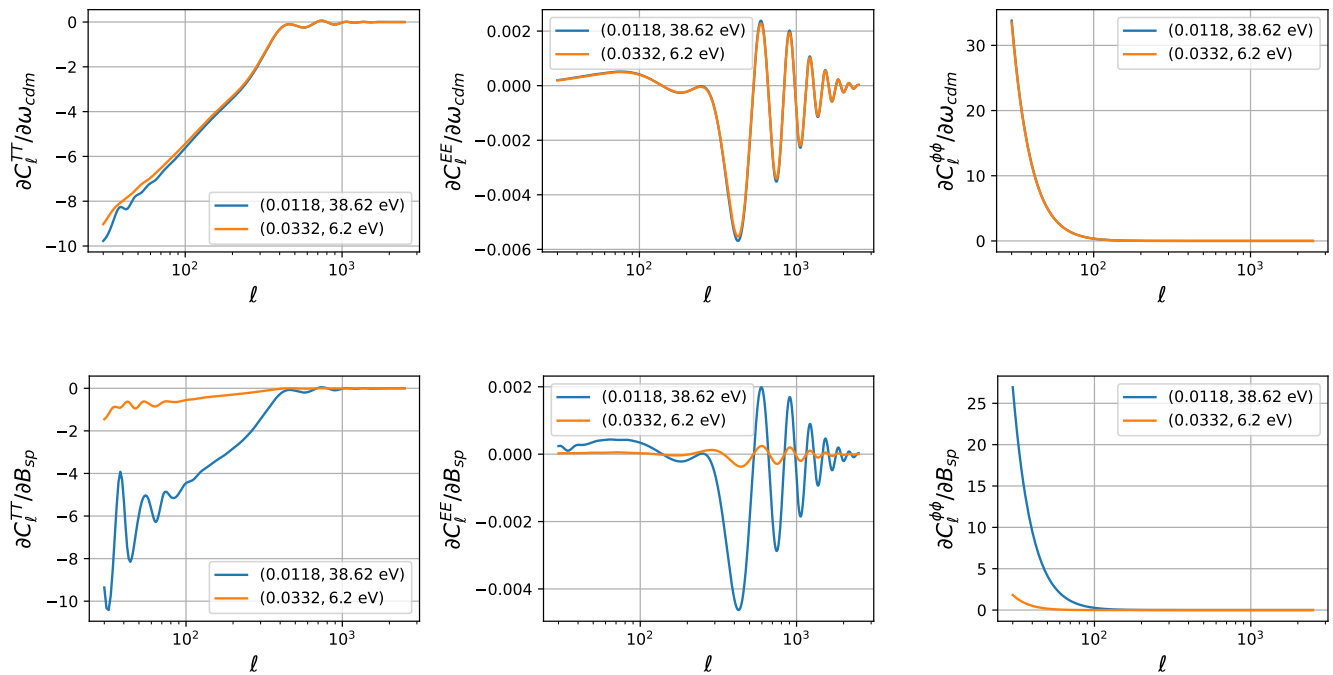


Figure 12: Comparative plots for the derivatives of the CMB primary and lensing power spectra with respect to  $\omega_{\text{cdm}}$  (top) and  $B_{\text{sp}}$  (bottom) for the NT model for the two sets of fiducial values.

Here  $\theta_0$  is the fiducial value of the parameter  $\theta$  under consideration and  $\Delta s$  is the step size. We have not accounted for the dependence of  $N_\ell^{\phi\phi}$  on the parameters (through the  $C_\ell$  values) while computing the derivatives;  $N_\ell^{\phi\phi}$ 's were kept fixed at their fiducial values.

Numerical derivatives play a crucial role in Fisher analysis, and in the computation of numerical derivatives, the choice of step sizes is important. Too large a step size misses fine features and introduces systematic errors while derivatives are prone to numerical noise and round off errors if the step size is too small. The step sizes used for the NT model are listed in Table VI. In Fig. 12, we compare the numerical derivatives of  $C_\ell^{TT}$ ,  $C_\ell^{EE}$ , and  $C_\ell^{\phi\phi}$  with respect to two parameters,  $\omega_{\text{cdm}}$  and  $B_{\text{sp}}$ , for both sets of fiducial values. We see that the derivatives with respect to  $\omega_{\text{cdm}}$  are nearly identical for both parameter sets. This observation holds for all the six  $\Lambda$ CDM parameters, which indicates that the direct effect of these parameters on the CMB spectra is dominant and largely independent of the specific LiMR properties. In contrast, the derivatives with respect to  $B_{\text{sp}}$  (and also  $m_{\text{sp}}$ ) are significantly different between the two parameter sets, which highlights the sensitivity of the CMB power spectra to the LiMR properties, like its branching ratio and its mass. Computationally, this is the primary source of the difference in the uncertainty values in  $\Delta N_{\text{eff}}$

and  $M_{\text{sp}}^{\text{eff}}$  between the two sets of fiducial values for the NT model. Similar arguments hold for the DW model.

Parameter	Fid. val. Set I		Fid. val. Set II	
	fiducial	step	fiducial	step
$\omega_b$	0.02247	1.6%	0.02242	5%
$\omega_{\text{cdm}}$	0.111	4%	0.120	4%
$h$	0.6804	1%	0.6711	3%
$10^9 A_s$	2.099	1%	2.110	1%
$n_s$	0.9661	1%	0.9652	1%
$\tau_{\text{reio}}$	0.0536	4%	0.0560	4%
$B_{\text{sp}}$	0.0118	1.6%	0.0332	9.6%
$m_{\text{sp}} [\text{eV}]$	38.62	8%	6.2	6%

Table VI: Fiducial values and step sizes (reported as percentage of fiducial value) for the six  $\Lambda$ CDM parameters and the NT model parameters used in the Fisher analysis for the two sets of fiducial values considered in the text.

- [1] Z. Hou, R. Keisler, L. Knox, M. Millea, and C. Reichardt, How massless neutrinos affect the cosmic microwave background damping tail, *Physical Review D* **87**, [10.1103/physrevd.87.083008](#) (2013).
- [2] B. Follin, L. Knox, M. Millea, and Z. Pan, First detection of the acoustic oscillation phase shift expected from the cosmic neutrino background, *Physical Review Letters* **115**, [10.1103/physrevlett.115.091301](#) (2015).
- [3] D. Baumann, D. Green, J. Meyers, and B. Wallisch, Phases of new physics in the cmb, *Journal of Cosmology and Astroparticle Physics* **2016** (01), 007–007.
- [4] J. Lesgourgues and S. Pastor, Neutrino mass from cosmology, *Advances in High Energy Physics* **2012**, 1–34 (2012).
- [5] N. Aghanim *et al.* (Planck), Planck 2018 results. VI. Cosmological parameters, *Astron. Astrophys.* **641**, A6 (2020), [Erratum: *Astron. Astrophys.* 652, C4 (2021)], [arXiv:1807.06209 \[astro-ph.CO\]](#).
- [6] E. Calabrese *et al.*, *The atacama cosmology telescope: Dr6 constraints on extended cosmological models* (2025), [arXiv:2503.14454 \[astro-ph.CO\]](#).
- [7] K. Akita and M. Yamaguchi, A precision calculation of relic neutrino decoupling, *Journal of Cosmology and Astroparticle Physics* **2020** (08), 012–012.
- [8] J. Froustey, C. Pitrou, and M. C. Volpe, Neutrino decoupling including flavour oscillations and primordial nucleosynthesis, *Journal of Cosmology and Astroparticle Physics* **2020** (12), 015–015.
- [9] J. J. Bennett, G. Buldgen, P. F. de Salas, M. Drewes, S. Gariazzo, S. Pastor, and Y. Y. Wong, Towards a precision calculation of the effective number of neutrinos  $n_{\text{eff}}$  in the standard model. part ii. neutrino decoupling in the presence of flavour oscillations and finite-temperature qcd, *Journal of Cosmology and Astroparticle Physics* **2021** (04), 073.
- [10] A. G. Adame, J. Aguilar, S. Ahlen, S. Alam, D. M. Alexander, M. Alvarez, O. Alves, A. Anand, U. Andrade, E. Armengaud, *et al.*, Desi 2024 vi: cosmological constraints from the measurements of baryon acoustic oscillations, *Journal of Cosmology and Astroparticle Physics* **2025** (02).
- [11] W. Elbers *et al.*, *Constraints on neutrino physics from desi dr2 bao and dr1 full shape* (2025), [arXiv:2503.14744 \[astro-ph.CO\]](#).
- [12] K. N. A. *et al.*, *Cmb-s4 science book, first edition* (2016), [arXiv:1610.02743 \[astro-ph.CO\]](#).
- [13] K. Abazajian, G. M. Fuller, and M. Patel, Sterile neutrino hot, warm, and cold dark matter, *Physical Review D* **64**, [10.1103/physrevd.64.023501](#) (2001).
- [14] A. Boyarsky, O. Ruchayskiy, and M. Shaposhnikov, The role of sterile neutrinos in cosmology and astrophysics, *Annual Review of Nuclear and Particle Science* **59**, 191–214 (2009).
- [15] K. N. Abazajian *et al.*, *Light sterile neutrinos: A white paper* (2012), [arXiv:1204.5379 \[hep-ph\]](#).
- [16] C. Brust, D. E. Kaplan, and M. T. Walters, New light species and the cmb, *Journal of High Energy Physics* **2013**, [10.1007/jhep12\(2013\)058](#) (2013).
- [17] A. Salvio, A. Strumia, and W. Xue, Thermal axion production, *Journal of Cosmology and Astroparticle Physics* **2014** (01), 011–011.
- [18] M. Kawasaki, M. Yamada, and T. T. Yanagida, Observable dark radiation from a cosmologically safe qcd axion, *Physical Review D* **91**, [10.1103/physrevd.91.125018](#) (2015).
- [19] D. Baumann, D. Green, and B. Wallisch, New target for cosmic axion searches, *Physical Review Letters* **117**, [10.1103/physrevlett.117.171301](#) (2016).
- [20] C. Giunti and M. Laveder, 3+1 and 3+2 sterile neutrino fits, *Phys. Rev. D* **84**, 073008 (2011).
- [21] J. M. Conrad, C. M. Ignarra, G. Karagiorgi, M. H. Shaevitz, and J. Spitz, *Sterile neutrino fits to short baseline neutrino oscillation measurements* (2012), [arXiv:1207.4765 \[hep-ex\]](#).
- [22] S. Gariazzo, C. Giunti, M. Laveder, and Y. F. Li, Updated global 3+1 analysis of short-baseline neutrino oscillations, *Journal of High Energy Physics* **2017**, [10.1007/jhep06\(2017\)135](#) (2017).
- [23] A. Aguilar, L. B. Auerbach, R. L. Burman, D. O. Caldwell, E. D. Church, A. K. Cochran, J. B. Donahue, A. Fazely, G. T. Garvey, R. M. Gunasingha, R. Im-lay, W. C. Louis, R. Majkic, A. Malik, W. Metcalf, G. B. Mills, V. Sandberg, D. Smith, I. Stancu, M. Sung, R. Tayloe, G. J. VanDalen, W. Vernon, N. Wadia, D. H. White, and S. Yellin, Evidence for neutrino oscillations from the observation of electron anti-neutrinos in a muon anti-neutrino beam, *Physical Review D* **64**, [10.1103/physrevd.64.112007](#) (2001).
- [24] A. A. Aguilar-Arevalo, B. Brown, L. Bugel, G. Cheng, J. Conrad, R. Cooper, R. Dharmapalan, A. Diaz, and Z. D. *et al.* (MiniBooNE Collaboration), Significant excess of electronlike events in the miniboone short baseline neutrino experiment, *Physical Review Letters* **121**, [10.1103/physrevlett.121.221801](#) (2018).
- [25] N. Arkani-Hamed, T. Cohen, R. T. D’Agnolo, A. Hook, H. D. Kim, and D. Pinner, Solving the Hierarchy Problem at Reheating with a Large Number of Degrees of Freedom, *Phys. Rev. Lett.* **117**, 251801 (2016), [arXiv:1607.06821 \[hep-ph\]](#).
- [26] A. Banerjee, B. Jain, N. Dalal, and J. Shelton, Tests of Neutrino and Dark Radiation Models from Galaxy and CMB surveys, *JCAP* **01**, 022, [arXiv:1612.07126 \[astro-ph.CO\]](#).
- [27] B. Wallisch, *Cosmological Probes of Light Relics*, Ph.D. thesis, University of Cambridge (2018).
- [28] S. Bashinsky and U. Seljak, Signatures of relativistic neutrinos in cmb anisotropy and matter clustering, *Physical Review D* **69**, [10.1103/physrevd.69.083002](#) (2004).
- [29] D. Green *et al.*, *Messengers from the early universe: Cosmic neutrinos and other light relics* (2019), [arXiv:1903.04763 \[astro-ph.CO\]](#).
- [30] Z. Pan and L. Knox, Constraints on neutrino mass from cosmic microwave background and large-scale structure, *Monthly Notices of the Royal Astronomical Society* **454**, 3200–3206 (2015).
- [31] J. Lesgourgues, G. Mangano, G. Miele, and S. Pastor, *Neutrino Cosmology* (Cambridge University Press, 2013).
- [32] W. L. Xu, J. B. Muñoz, and C. Dvorkin, Cosmological constraints on light but massive relics, *Physical Review D* **105**, [10.1103/physrevd.105.095029](#) (2022).
- [33] N. DePorzio, W. L. Xu, J. B. Muñoz, and C. Dvorkin, Finding ev-scale light relics with cosmological ob-

- servables, *Physical Review D* **103**, [10.1103/physrevd.103.023504](https://arxiv.org/abs/10.1103/physrevd.103.023504) (2021).
- [34] S. Dodelson and L. M. Widrow, Sterile neutrinos as dark matter, *Physical Review Letters* **72**, 17–20 (1994).
- [35] X. Shi and G. M. Fuller, New dark matter candidate: Nonthermal sterile neutrinos, *Phys. Rev. Lett.* **82**, 2832 (1999).
- [36] A. Cuoco, J. Lesgourgues, G. Mangano, and S. Pastor, Do observations prove that cosmological neutrinos are thermally distributed?, *Physical Review D* **71**, [10.1103/physrevd.71.123501](https://arxiv.org/abs/10.1103/physrevd.71.123501) (2005).
- [37] J. P. Conlon and M. C. D. Marsh, The Cosmophenomenology of Axionic Dark Radiation, *JHEP* **10**, 214, [arXiv:1304.1804 \[hep-ph\]](https://arxiv.org/abs/1304.1804).
- [38] J. Hasenkamp and J. Kersten, Dark radiation from particle decay: cosmological constraints and opportunities, *Journal of Cosmology and Astroparticle Physics* **2013** (08), 024–024.
- [39] B. S. Acharya, M. Dhuria, D. Ghosh, A. Maharana, and F. Muia, Cosmology in the presence of multiple light moduli, *Journal of Cosmology and Astroparticle Physics* **2019** (11), 035–035.
- [40] S. Bhattacharya, S. Das, K. Dutta, M. R. Gangopadhyay, R. Mahanta, and A. Maharana, Nonthermal hot dark matter from inflaton or moduli decay: Momentum distribution and relaxation of the cosmological mass bound, *Phys. Rev. D* **103**, 063503 (2021), [arXiv:2009.05987 \[astro-ph.CO\]](https://arxiv.org/abs/2009.05987).
- [41] V. Mukhanov, *Physical Foundations of Cosmology* (Cambridge University Press, 2005).
- [42] M. Cicoli, K. Dutta, A. Maharana, and F. Quevedo, Moduli vacuum misalignment and precise predictions in string inflation, *Journal of Cosmology and Astroparticle Physics* **2016** (08), 006–006.
- [43] M. A. Acero and J. Lesgourgues, Cosmological constraints on a light nonthermal sterile neutrino, *Physical Review D* **79**, [10.1103/physrevd.79.045026](https://arxiv.org/abs/10.1103/physrevd.79.045026) (2009).
- [44] M. Tegmark, A. N. Taylor, and A. F. Heavens, Karhunen-loeve eigenvalue problems in cosmology: How should we tackle large data sets?, *The Astrophysical Journal* **480**, 22–35 (1997).
- [45] D. Coe, *Fisher matrices and confidence ellipses: A quick-start guide and software* (2009), [arXiv:0906.4123 \[astro-ph.IM\]](https://arxiv.org/abs/0906.4123).
- [46] W. L. K. Wu, J. Errard, C. Dvorkin, C. L. Kuo, A. T. Lee, P. McDonald, A. Slosar, and O. Zahn, A guide to designing future ground-based cosmic microwave background experiments, *The Astrophysical Journal* **788**, 138 (2014).
- [47] A. Manzotti, S. Dodelson, and Y. Park, External priors for the next generation of cmb experiments, *Physical Review D* **93**, [10.1103/PhysRevD.93.063009](https://arxiv.org/abs/10.1103/PhysRevD.93.063009) (2016).
- [48] D. Blas, J. Lesgourgues, and T. Tram, The cosmic linear anisotropy solving system (class). part ii: Approximation schemes, *Journal of Cosmology and Astroparticle Physics* **2011** (07), 034–034.
- [49] J. Lesgourgues and T. Tram, The cosmic linear anisotropy solving system (class) iv: efficient implementation of non-cold relics, *Journal of Cosmology and Astroparticle Physics* **2011** (09), 032–032.
- [50] Z. Li, V. Gluscevic, K. K. Boddy, and M. S. Madhavacheril, Disentangling dark physics with cosmic microwave background experiments, *Physical Review D* **98**, [10.1103/physrevd.98.123524](https://arxiv.org/abs/10.1103/physrevd.98.123524) (2018).
- [51] M. S. Madhavacheril and J. C. Hill, Mitigating foreground biases in cmb lensing reconstruction using cleaned gradients, *Physical Review D* **98**, [10.1103/physrevd.98.023534](https://arxiv.org/abs/10.1103/physrevd.98.023534) (2018).
- [52] A. Manzotti, S. Dodelson, and Y. Park, External priors for the next generation of cmb experiments, *Physical Review D* **93**, [10.1103/physrevd.93.063009](https://arxiv.org/abs/10.1103/physrevd.93.063009) (2016).
- [53] S. Das, A. Maharana, V. Poulin, and R. K. Sharma, Nonthermal neutrino-like hot dark matter in light of the S8 tension, *Phys. Rev. D* **105**, 103503 (2022), [arXiv:2104.03329 \[astro-ph.CO\]](https://arxiv.org/abs/2104.03329).
- [54] N. Sehgal *et al.*, *Cmb-hd: Astro2020 rfi response* (2020), [arXiv:2002.12714 \[astro-ph.CO\]](https://arxiv.org/abs/2002.12714).
- [55] D. Baumann, D. Green, and B. Wallisch, Searching for light relics with large-scale structure, *Journal of Cosmology and Astroparticle Physics* **2018** (08), 029–029.
- [56] A. Banerjee, S. Das, A. Maharana, and R. Kumar Sharma, Signatures of Light Massive Relics on non-linear structure formation, *Mon. Not. Roy. Astron. Soc.* **516**, 2038 (2022), [arXiv:2202.09840 \[astro-ph.CO\]](https://arxiv.org/abs/2202.09840).